Locomotive Micro-Implant with Active Electromagnetic Propulsion

Daniel Pivonka, Ada S. Y. Poon, and Teresa H. Meng
Electrical Engineering
Stanford University
{*pivonka,adapoon,thm*}*@stanford.edu*

Abstract

An active locomotive technique requiring only an external power source and a static magnetic field is presented, and its operation is analyzed and simulated. For a modest static MRI magnetic field of 1 T, the results show that a 1-mm cube achieves roughly 3 cm/sec of lateral motion using less than 20.4 μW of power. Current-carrying wires generate the forces, resulting in highly controllable motion. Existing solutions trade off size and power: passive solutions are small but impractical, and mechanical solutions are inefficient and large. The presented solution captures the advantages of both systems, and has much better scalability.

1. Introduction

Locomotive implantable devices have numerous applications including sensing, imaging, minimally invasive surgery, and research. Many techniques have been used to generate motion, including mechanical solutions [1], [2], [3] and passive magnetic solutions [1], [4], [5]. Power sources dominate the size of existing active implant technologies, and this size constaint (typically in the cm-range) limits the potential for propulsion. Additionally, mechanical propulsion is inherently inefficient at the scale of interest. Passive locomotion schemes have circumvented the power and efficiency issues, but require large field gradients and usually cannot generate vertical motion. Recent improvements in wireless power transmission efficiency allow for mm-sized implants to receive on the order of 150 μW at a depth of 2 cm [6]. With this technology, a new device can exploit the advantages of both approaches. A low-power method for controlling the motion of such implants can enhance functionality for a variety of applications, and this paper discusses a technique that accomplishes this goal using available clinical technologies.

The proposed electromagnetic propulsion technique is a simple application of the Lorentz force on specific wire arrangements. In addition to forward propulsion, these wire arrangements can generate torques to steer the device through the fluid. Although the magnetic field only exerts perpendicular forces on the wires, altering the orientation of the device can generate lift due to the fluid drag force, resulting in vertical motion. To fully realize the forces and torques necessary for this control, DC magnetic shielding must be used to prevent certain currents from experiencing forces. In this way, the design achieves full 3D motion by a simple manipulation of currents.

The organization of the paper is as follows. Section 2 analyzes the thrust forces generated in static magnetic fields. A current loop that achieves forward motion is analyzed, and the motion in water is predicted. Additionally, the effects of scaling the device are presented to show the versatility of active electromagnetic propulsion. Section 3 verifies the theoretical results through fluid simulations, and shows the scalability of the design. The performance is contrasted with competing methods in Section 4, and the advantages of new design are emphasized. Finally, the paper is concluded in Section 5.

2. Theoretical Model

The theoretical model is separated into two parts: force generation and fluid motion. For the purposes of this analysis, buoyant forces and gravitational forces are not considered. The force $\mathbf{F}$ on a current-carrying wire is simply

$$\mathbf{F} = I\,\mathbf{L} \times \mathbf{B}, \tag{1}$$

where I is the current in the wire, $\mathbf{L}$ is a vector denoting the length and direction of the wire, and $\mathbf{B}$ is the magnetic field. This force is always perpendicular to the magnetic field, and is maximized when the wire orientation is perpendicular to the field. To generate a forward force with a loop of wire, the return path for the

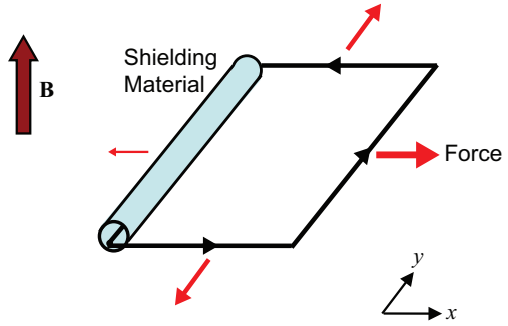

Figure 1: Current loop generating a forward force

current must be shielded from the magnetic field. A diagram depicting this arrangement is shown in Figure 1. The forces in the y-direction cancel, and the net force in the x-direction is

$$F = (1-\alpha)ILB, \tag{2}$$

where α represents the attenuation of the field inside the shielding material. When α is zero, the shielding is perfect and the wire inside the shielding material exerts no force on the device. Maximizing the force can be accomplished by maximizing I and L. The power consumption P of the main force generating wire is

$$P = I^2R = I^2\rho_c\frac{L}{A_w}, \tag{3}$$

where R is the resistance, ρ_c is the conductivity, and A_w is the cross-sectional area of the wire. The total power of the device is the sum of the power consumed by the wires. Equations (2) and (3) define the trade off between power consumption and the thrust force. Decreasing I and increasing L by the same factor results in the same force with less power usage. Also, increasing A_w reduces the required power. Therefore, the L and A_w should be maximized to achieve the best performance.

The thrust force works against the fluid drag force, which is velocity dependent. The dependence on velocity changes with the Reynolds number. The Reynolds number is given as

$$Re = \frac{\rho_f v D}{\mu}, \tag{4}$$

where ρ_f represents the density of the fluid, v is the velocity of the object, D is a characteristic dimension, and μ is the viscosity of the fluid. As the device becomes smaller, the Reynolds number decreases. For Reynolds numbers much greater than one (typically larger than 1000), the drag force D_1 can be written as

$$D_1 = \frac{1}{2}\rho_f v^2 A_f C_D, \tag{5}$$

where ρ_f is the density of the fluid, v is the velocity, A_f is the frontal area of the device, and C_D is the drag coefficient. When the two forces are equal, a steady-state velocity is reached. Combining equations (2), (3), and (5) yields the following result for the steady-state velocity:

$$\begin{aligned} v &= \sqrt{\frac{2(1-\alpha)LB}{\rho_f A_f C_D}}\sqrt{\frac{P}{R}} = \sqrt{\frac{2(1-\alpha)B}{\rho_f A_f C_D}}\sqrt[4]{\frac{LPA_w}{\rho_c}} \\ &\propto \sqrt{\frac{B}{A_f C_D}}\sqrt[4]{LPA_w}. \end{aligned} \tag{6}$$

Equation (6) reveals how the velocity changes with the relevant design parameters. The available power is proportional to the area of the device. Considering a cube with side length L, velocity varies inversely to the 4^{th} root of L. This means the velocity is relatively insensitive to changes in size. We also see that velocity varies with the square root of the magnetic field, which means it is relatively insensitive to the magnetic field as well.

As previously mentioned, this model is not valid for small Reynolds numbers. As the device is scaled down and the Reynolds number becomes small (less than 1), the fundamental fluid behavior follows Stokes Law. To greatly simplify the analysis, we will consider the behavior of a sphere even though this representation is not exact. For a sphere with radius r, the drag force in this regime is

$$D_2 = 6\pi\mu r v \tag{7}$$

with μ representing fluid viscosity and v representing velocity as before. To apply this equation to the presented design, we can approximate that $2r$ is roughly equal to L. If this equation for drag is combined with equations (2) and (3), the following is obtained for the velocity in the fluid:

$$\begin{aligned} v &= \frac{(1-\alpha)LB}{3\pi\mu L}\sqrt{\frac{P}{R}} = \frac{(1-\alpha)B}{3\pi\mu}\sqrt{\frac{PA_w}{L\rho_c}} \\ &\propto B\sqrt{\frac{PA_w}{L}}. \end{aligned} \tag{8}$$

In equation (8), we see that the variation of velocity with the relevant design parameters has fundamentally changed. Again, the available power is proportional to area, so the velocity varies with the square root of L, making it much more sensitive to size compared with the high Reynolds prediction. Also, velocity now decreases as size decreases. The magnetic field is directly proportional to the velocity, which shows that there is increased sensitivity to the field as well. It is important to note that neither equation (5) or (7) is valid when the Reynolds number does not fall into one of these extremes, and there is a transition period in between.

3. Simulations

Because the above theory only partially describes the behavior, it is necessary to run fluid simulations for an accurate depiction of performance. These simulations also serve to verify the theory. COMSOL was used to perform full simulations of the fluid mechanics. The device was approximated as a cube with side length L, and the drag force at a fixed velocity of 3 cm/sec was determined. This was done by fixing the object in space in a section of moving fluid, and then measuring the forces exerted on the object. An example simulation is shown in Figure 2. We then computed the necessary power to supply this force with equations (2) and (3). The plot in Figure 3 shows the theoretical power versus size at 3 cm/sec based on both the high and low Reynolds theory, as well as the result of the simulations. In this plot, the power is normalized to magnetic field squared. For the theoretical predictions, the drag coefficient C_D was assumed to be a constant equal to 1.05 for a cube, which is true for large Reynolds numbers.

At large sizes (and high Reynolds numbers), the simulation matches the predicted values very well. As the size is reduced, we see the transition to the low Reynolds number prediction. This prediction describes a sphere, and so there is some deviation. Additionally, C_D varies inversely with the Reynolds number, and this was not included in the model. The sizes of interest for medical implants are at or below the transition region, so simulations must be used to predict their behavior.

For a practical design, the limits of performance are determined by the available power and the external magnetic field. The size of the device determines how much power can be received from an external power source, and magnetic field depends only on the external transmitter. Because different applications have different requirements, it is of interest to determine what the limits of the design are. The theoretical models can not accurately predict these limits, and so again we rely on the fluid simulations. Figure 4 shows power as a function of the magnetic field and size at fixed velocities. The available power for a device can be estimated once the size and depth of the implant are known, and then the acheivable velocity can be estimated with Figure 4. As a simple example, consider the 1-mm cube analyzed above. At a depth of 2 cm, the available power is 150μW [6]. Now, we must divide this power among the wires. For forward movement, this can be accomplished with a loop with two long wires of length L and two very short wires connecting them. Therefore, we have roughly 75 μW of power available for the force generating wire, and from Figure 4 this corresponds to a velocity of approximately 7 cm/sec.

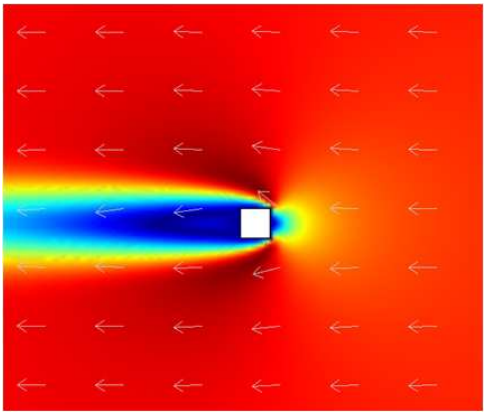

Figure 2: Example simulation for 1mm cube at 3 cm/sec

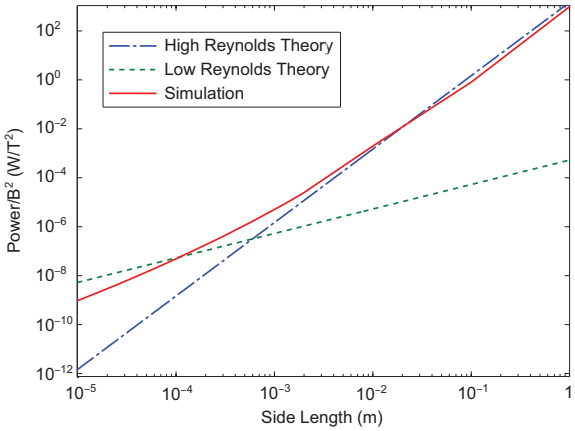

Figure 3: Required power as function of magnetic field and size

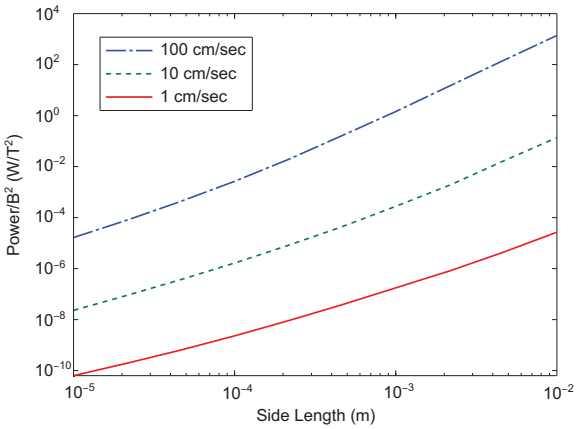

Figure 4: Required power for different velocities

4. Discussion

As mentioned in the introduction, there are two dominant competing methods for locomotive micro-implants. The first is a passive magnetic propulsion technique that exerts force on a small ferromagnetic material with magnetic field gradients, and the second consists of mechanical propulsion with active power. The passive propulsion method requires MRI because the gradient fields must be large and precisely controlled. The equation for the thrust force in this case is

$$\mathbf{F} = V_{ferro}(\mathbf{M} \cdot \nabla)\mathbf{B} \tag{9}$$

with $\mathbf{M}$ representing the magnetization of the ferromagnetic material, V_{ferro} representing the volume of the magnetic object, and $\mathbf{B}$ representing the magnetic field [4]. The gradient must be in the direction of movement, and even MRI cannot overcome the force of gravity for devices smaller than roughly 1 mm. The force scales poorly as the size is reduced because it is proportional to the volume of the object. From a practical perspective, generating large field gradients is complicated, and even current MRI technology is inadequate.

In addition to the passive method, it is also possible to use mechanical propulsion. Mechanical propulsion is accomplished with a wide variety of techniques. A few possible methods include flagella/motors, pumps, and acoustic streaming. These designs typically suffer from low conversion efficiency from input power to thrust, especially as the Reynolds number decreases. There are losses associated with the conversion from electrical power to mechanical motion, and more loss associated with the conversion from mechanical motion to forward thrust. As a result of the low efficiency, a fairly substantial amount of power is required, and the power source dominates the size making it difficult to miniaturize. Presently, most medical implants have no propulsion at all, such as GI tract imaging capsules.

Active electromagnetic propulsion has many advantages over these methods. It can efficiently generate thrust with a static magnetic field. The motion is highly controllable with simple manipulations of currents. Though it was not discussed in this paper, the gravitational forces can be balanced with buoyant forces with minor adjustments. Essentially, active electromagnetic propulsion offers the flexibility to meet the requirements of a variety of applications, whether they require small sizes or small magnetic fields.

In the theoretical analysis, we attempted to derive the scalability of the design and found that it there are two regions of operation. For large enough devices, the scaling occurs as predicted, but there is deviation as the size is reduced. The theoretical predictions could not accurately predict behavior in the transition region, and so simulations were necessary to complete the picture. Figure 3 shows that the actual scaling of the device is somewhere in between these two predictions. Power does not decrease as quickly with size as the high Reynolds model predicts, but decreases more quickly than the low Reynolds model predicts. Figure 4 shows the simulated scalability of the design at different sizes and speeds, which is useful for determining the feasibility of a given design.

5. Conclusion

Attempts at designing a locomotive micro implant with current technology have not resulted in an adequate design. Analysis of active electromagnetic propulsion shows significant enhancements over the current technology. This new method is efficient, controllable, and allows for flexibility in its design and use. Simulations show that a 1-mm cube can achieve a velocity of 3 cm/sec with less than 20.4 μW and a 1 T static field. Because of the way velocity scales with force and the magnetic field, the size of the device can be reduced more than any current technology. Such a device would be useful for a wide variety of applications, and could fundamentally change many medical procedures.

References

[1] J.Abbott, "Robotics in the small part I: Microrobotics," *IEEE Robotics and Automation Magazine*, pp. 92–103, June 2007.

[2] H. Li, G. Yan, and G. Ma, "An active endoscopic robot based on wireless power transmission and electromagnetic localization," *Int. J. Med. Robotics Comput. Assist. Surg.*, vol. 4, pp. 355–367, 2008.

[3] B. Lenarts and R. Puers, "An inductive power link for a wireless endoscope," *Biosensors and Bioelectronics*, vol. 22, pp. 1390–1395, 2007.

[4] J. B. Mathieu, G. Beaudoin, and S. Martel, "Method of propulsion of a ferromagnetic core in the cardiovascular system through magnetic gradients generated by an MRI system," *IEEE Trans. Biomed. Eng.*, vol. 53, no. 2, pp. 292–299, Feb. 2006.

[5] J. Abbott, O. Ergeneman, M. P. Kummer, A. M. Hirt, and B. J. Nelson, "Modeling magnetic torque and force for controlled manipulation of soft-magnetic bodies," *IEEE Trans. Robotics*, vol. 23, no. 6, pp. 1247–1252, Dec. 2007.

[6] A. S. Y. Poon, S. O'Driscoll, and T. H. Meng, "Optimal operating frequency in wireless power transmission for implantable devices," *Proc. IEEE Engineering in Medicine and Biology Society Annual Intl. Conference (EMBC), Lyon, France*, pp. 5673–5678, Aug. 2007.